σ Bonds: Electronic structure, photophysics, and photochemistry of oligosilanes*

Heather A. Fogarty, Deborah L. Casher, Roman Imhof, Thorsten Schepers, David W. Rooklin, and Josef Michl[‡]

Department of Chemistry and Biochemistry, University of Colorado, Boulder, CO 80309-0215, USA

Abstract: The making and breaking of σ bonds is an integral part of almost all photochemical reactions. Yet, the electronic states of σ electrons are not nearly as well understood as the states of π-electron systems. Efforts in our laboratory to enhance the current state of their understanding are described, using the specific example of oligosilanes. We address the intrinsically cyclic nature of σ delocalization and its dependence on chain length and conformation, both in terms of theory and spectroscopic experiments, from the simplest disilane chromophore to the spectral properties of the individual conformers of permethylated heptasilane. We also describe a new low-energy luminescence from certain conformers of permethylated oligosilanes.

INTRODUCTION

Electronic states of σ bonds in main-group molecules have not received much attention from photochemists and photophysicists. We argue that they deserve to be better understood, and provide a rationale for our choice of Si–Si bonds for a detailed study. We first describe the spectroscopic properties of a single such bond in hexaalkyldisilanes, and then address bond–bond interactions that lead to σ delocalization. Specifically, we deal with the effects of chain length and conformation on the excited singlet states of permethylated saturated oligosilanes.

ELECTRONIC STATES OF σ BONDS AND MAIN-GROUP PHOTOCHEMISTRY

Covalent σ bonds are the glue that holds together molecules composed of atoms of main-group elements and, in particular, all organic molecules. A few of the valence electrons may be in nonbonding lone pairs or in π bonds, but most of the bonds are of the σ type even in such highly unsaturated species as graphite (75 %) and acetylene (60 %). Almost all reactions of main-group element molecules involve the making or breaking of a σ bond. With the exceptions of E-Z isomerization around double bonds, π-electron valence tautomerization as in cyclobutadiene, and some electron-transfer reactions, it is hard to think of reactions in which one or more σ bonds are not made, broken, or both. This is seen in ground-state as well as excited-state reactions, and it is clearly apparent in their orbital correlation diagrams. It is common for state correlation diagrams of the Woodward–Hoffmann or Salem types to refer to states described by excitation from or into orbitals of σ symmetry, yet the nature and even the energy of such states are often somewhat or entirely mysterious. We have all shown our students the orbital, configuration, and state correlation diagrams for the 2s+2s cycloaddition of two ethylene mole-

cules to cyclobutane and explained in some detail the nature and energy of the excited states of ethylene; what did we tell them about the excited states of cyclobutane?

Because of the transmission properties of air and common solvents, organic photochemists rarely work with light of wavelengths that would cause σσ* excitations. Our reactants typically contain molecular regions with π or lone-pair electrons, and initial excitation is usually into ππ*, nπ*, and occasionally into nσ* or Rydberg states, which can be reached with light of longer wavelengths than typical σσ* states. In effect, this initial excitation is merely a stepping stone for translocation of the initially ππ*, nπ*, or similar electronic excitation energy to a nearby σ bond that will be broken or made. This process usually takes time, permitting internal conversion to the lowest excited state of the initial multiplicity and vibrational equilibration to take place, and Kasha's rule follows. One would not expect this rule to hold very well if the initial excitation involved directly the bond to be broken.

It is possible to discern an analogy in the photochemistry of transition-metal compounds, where low-energy d-d excitation tends to play the role of an initial stepping stone, whereas the excitation of the dative bonds to ligands at higher energies delivers energy directly to bonds to be broken and frequently violates Kasha's rule. In this case, both types of excitation can typically be accomplished with light of wavelengths longer than 200 nm, and indeed, Kasha's rule is often not invoked in the photochemistry of transition-metal compounds.

In the currently usual description of photochemical processes in terms of potential energy diagrams, the process of excitation energy flow into the bonds to be broken and to be made corresponds to the motion of the initially excited wave packet (or, more simply, point) from vertical (Franck–Condon) geometries to biradicaloid geometries at which conical intersections (funnels) occur, and which almost always involve excitations of σ bonds. Qualitatively, it is often useful to start an analysis with zero-order states such as ππ* and σσ*, whose crossing produces barriers and intersections, and only subsequently consider their interactions, which modify the barriers, but usually do not remove them completely [1]. The remaining barriers separating the Franck–Condon region from the point of return to the ground state are then responsible for the time lapse between the initial excitation and product formation and the resulting Kasha's rule. The effect of the small barriers in excited-state potential energy surfaces can be dramatic; e.g., at very low temperatures, dewar naphthalene tunnels out of a local minimum in the lowest excited singlet state with a rate constant of only 4×10^7 s^{-1}, competitive with fluorescence and intersystem crossing, although its conversion to ground-state naphthalene is exothermic by ~150 kcal/mol [2].

Clearly, it would be useful if we knew more about the excited states of collections of interacting σ bonds and could draw their potential energy levels with the confidence that we feel when we deal with excited states of π systems. There are at least three reasons why our knowledge is very limited: (i) Spectroscopic studies in the vacuum UV region are technically difficult for reasons such as lack of suitable solvents for low-volatility materials, and are faced with complications, such as the presence of numerous states of similar energies (including Rydberg states) and the diffuse nature of most absorption bands (related to their directly dissociative nature). (ii) Computational studies are difficult for many of the same reasons (high density of states, mixing of valence and Rydberg states) and their results are difficult to compare with experiments, making their pursuit unattractive. (iii) Excited states of σ-bonded systems are much more complicated than those of π systems and not nearly as amenable to simplified qualitative descriptions. Compare, for instance, the relative simplicity of the ππ* states of a linear polyene, H–(CH=CH)$_n$–H, characterized by a one-dimensional topology of a linearly interacting set of p orbitals, with the complexity of the σσ* states expected for a random conformation of an H–(CH$_2$)$_n$–H alkane, which offers the possibility of excitation from C–C as well as C–H σ bonds, and in which each of the four valence orbitals on each carbon has significant interactions with two or more valence orbitals on each neighboring carbon, not to mention the interactions with hydrogen orbitals.

Little wonder, then, that only the excited states of the smallest saturated molecules are understood in any detail, that the weak fluorescence of saturated hydrocarbons, discovered decades ago [3], remains unassigned to this day, and that we are reduced to hand-waving when describing one side of the two

ethylenes - cyclobutane correlation diagram. Chipping away at this block of ignorance, by whatever means available, seems like a worthwhile task.

Si–Si BONDS

There is considerable similarity between hydrocarbons and their silicon analogs; indeed, their Lewis structures look identical. Although Si–Si bonds are generally slightly weaker, the ground states of C_nH_{2n+2} and Si_nH_{2n+2} resemble each other strongly (e.g., in terms of valence angles and conformational preferences). There are some obvious differences, in that silicon tolerates divalency much better than carbon and makes much weaker π bonds than carbon. Also, unlike carbon, silicon is much more electropositive than hydrogen, imparting a clearly polar character to Si–H bonds. However, since the underlying interactions of valence orbitals are indisputably qualitatively similar, a study of oligosilanes will teach us something about σ-bonded systems in general. This belief is illustrated by the popularity that the very qualitative Sandorfy models of electronic structure of saturated systems, originally devised for alkanes [4], have had among photophysicists investigating polysilanes [5]. In these models, the basis set of valence orbitals is taken to consist of sp^3 hybrids on the backbone atoms and ls orbitals on the hydrogen substituents, making the analogy between carbon and silicon particularly clear (see below for additional detail).

At the risk of imitating the person who lost a coin in a dark corner and is looking for it under a street light, because that is where it would be more likely to be visible, we have been examining the spectroscopy and photophysics of oligosilanes rather than hydrocarbons, because it is much easier and will still teach us something useful about σ systems. Of course, the photophysics and photochemistry of silicon compounds and particularly of polysilanes are of considerable interest in themselves [5,6]. After all, the first direct observation of organic silylenes [7] and the first syntheses of compounds with Si=Si [8] and Si=C [9] double bonds were photochemical, polysilanes have been examined as photo-resists [10], have high photoconductivity [11], interesting nonlinear optical properties [12], etc. As is customary, we work with the much more stable peralkylated oligosilanes Si_nR_{2n+2} and not the parent Si_nH_{2n+2} compounds.

There are two primary reasons why the study of oligosilanes is easier: (i) The excitation energies are lower. The lowest singlet excited states generally occur at wavelengths longer than 200 nm, and certain conformations of fully saturated alkylated polysilanes absorb close to 400 nm [13]. The much lower singlet σσ* excitation energy of the $Me_3Si–SiMe_3$ bond relative to the $Me_3C–CMe_3$ bond, which has nearly equal strength, can be very qualitatively understood as due to the electropositive nature of silicon [14]. In the first approximation, the dissociation limits are $Me_3Si^+ + {}^-SiMe_3$ and $Me_3C^+ + {}^-CMe_3$, respectively, with the former clearly much lower in energy relative to the equilibrium ground state. Even though the C–C bond is shorter than Si–Si, the gain in electrostatic energy upon building the molecule from the dissociation fragments is not sufficiently larger for $Me_3C^+ + {}^-CMe_3$, whose positive charge is considerably delocalized into the methyl groups. (ii) The spectrum is simpler, since only excitations from Si–Si orbitals occur at low energies, and excitations from Si–H or Si–C bonds can be ignored. This, too, is a consequence of the electropositive nature of silicon. The Si–H (or Si–C) bond orbitals are polarized toward the more electronegative H (or C) atom and lie well below the Si–Si orbitals. By the same token, the Si–H (or Si–C) antibonding orbitals are polarized toward the Si atom. As a result, low-energy excitation tends to concentrate on the backbone. A similar situation occurs in fluorocarbons, but their excitation energies are much higher [15].

ELECTRONIC STATES OF A LONE Si–Si BOND

The structures of the silicon compounds **1–21** that will be referred to below are collected in Chart 1. Figure 1 shows the several lowest ionization potentials of Si_2Me_6 (**1**) and Si_2t-Bu_6 (**2**), along with the calculated occupied Si–Si and Si–C Kohn-Sham orbital energies [B3LYP/6-31G(d,p)] [16]. A constant
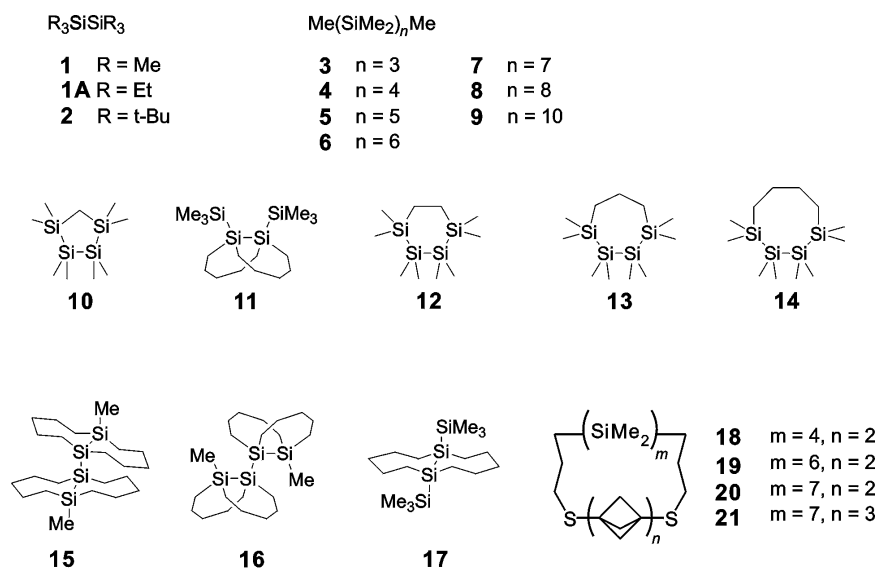
R₃SiSiR₃ — rendered as R_3SiSiR_3

R_3SiSiR_3 $Me(SiMe_2)_nMe$

1   R = Me   **3**   n = 3   **7**   n = 7
1A R = Et   **4**   n = 4   **8**   n = 8
2   R = t-Bu   **5**   n = 5   **9**   n = 10
                6   n = 6

10   **11**   **12**   **13**   **14**

15   **16**   **17**

18   m = 4, n = 2
19   m = 6, n = 2
20   m = 7, n = 2
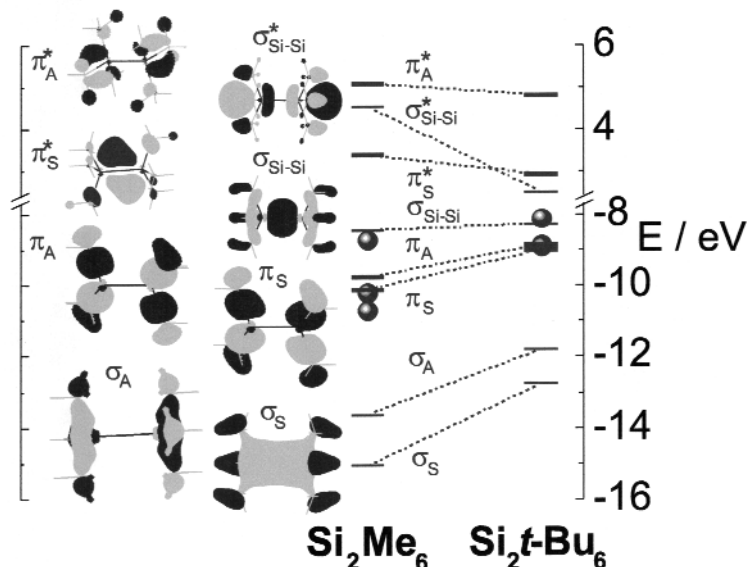**21**   m = 7, n = 3

Chart 1

Fig. 1 Observed (circle) negative ionization potential and calculated [bar; B3LYP/6-31G(d,p)//MP2/VTZ] occupied and virtual MO energies of disilanes **1** and **2**. Only selected molecular orbitals of **1** are illustrated. They are Si–C orbitals unless labeled Si–Si. Thicker bars indicate doubly degenerate orbitals.

value of 2.0 eV was added to each orbital energy to correct roughly for the inadequacy of Koopmans' approximation [17]. The figure also shows the energies of a few virtual orbitals, and simplified drawings of the bonding and antibonding orbitals associated with these bonds. It illustrates the above statement that the σ_{Si-Si} orbital, localized on the silicon atoms, is at higher energy than the σ orbitals used to attach lateral substituents, and is the only one that low-energy excitations will start from. Because of the three-fold symmetry, the lateral σ orbitals are organized in a pair of degenerate higher-energy orbitals with a nodal plane containing the Si–Si bond, and a pair of lower-energy nondegenerate orbitals.

Although all these orbitals are built from Si–C σ-bond orbitals, the former are of π symmetry relative to the three-fold axis, and will be referred to as π_{Si-C} orbitals. The latter pair of nondegenerate Si–C orbitals is of σ symmetry. The zero-order σ_{Si-Si} orbital and the in-phase combination of symmetrically combined σ_{Si-C} orbitals interact and mix.

The σ_{Si-C} orbitals, and to a lesser extent the π_{Si-C} orbitals, are at substantially higher energies in **2** than in **1**. The larger number of C–C and C–H bonding orbitals in **2** interact with the Si–C bond orbitals, of both symmetries, and push up their energy. Otherwise expressed, the general increase in the energies of the bonding orbitals in the series Si_2Me_6 to Si_2t-Bu_6 is due to the inductive effect of the large polarizable substituents [18,19].

Each pair of π_{Si-C} or σ_{Si-C} orbitals consists of a lower-energy in-phase (symmetric, S) and a higher-energy out-of-phase (anti-symmetric, A) combination of Si–C group orbitals of the trialkylsilyl radicals. Because the Si–Si distance is considerable (normally ~2.35 Å), their interaction is relatively weak and the splitting is small. This is especially apparent in the case of Si_2t-Bu_6, whose Si–Si bond is 2.70 Å long.

Antibonding orbitals are not revealed in a photoelectron spectrum, but computational results suggest that they are quite analogous to the bonding ones (Fig. 1). A σ^*_{Si-Si} orbital is localized on the silicon atoms and has a node across the Si–Si bond. The π^*_{Si-C} orbitals consist of two degenerate pairs with the lower-energy pair being in-phase (S) and the higher energy pair out-of-phase (A). The π^*_{Si-C} orbitals have their amplitude concentrated on the C atoms, located far apart, while the π^*_{Si-C} orbital amplitude is mostly on the Si atoms that are neighbors, and this causes a greater splitting of the π^*_{Si-C} orbitals. In Si_2Me_6, the in-phase (S) pair of π^*_{Si-C} orbitals is lower in energy than the σ^*_{Si-Si} orbital, while in Si_2t-Bu_6 the order is the opposite. This trend was also derived from calculations performed on Si_2Me_6 as a function of the Si–Si bond length [19]; the energies of the Si–Si σ bonding and antibonding orbitals approach each other as the Si–Si bond is stretched, whereas the energies of the π^*_{Si-C} orbitals do not change much. The S and A σ^*_{Si-C} orbitals are even a little higher in energy and mix heavily with others.

One would expect two low-lying optically allowed excitations from the σ_{Si-Si} orbital, a degenerate σπ* excitation polarized perpendicular to the Si–Si bond and a nondegenerate σσ* excitation polarized parallel to the Si–Si bond. Upon Si–Si bond stretching, the latter should drop faster in energy than the former. Figure 2 compares the absorption and magnetic circular dichroism (MCD) spectra of Si_2Me_6 (**1**), Si_2Et_6 (**1A**), and Si_2t-Bu_6 (**2**). The relatively weak absorption band that appears in the first two spectra clearly belongs to a degenerate transition since it corresponds to an S-shaped curve in the MCD spectrum, and is assigned to the σπ* transition. In **1**, there is no sign of the σσ* transition, which lies at a higher energy, above the experimental window. In **1A**, the onset of the σσ* transition is barely observable. However, in the spectrum of Si_2t-Bu_6, the σπ* transition appears only as a shoulder on the side of a much stronger band, which is assigned to the σσ* transition, brought into the observed range because of the much longer Si–Si bond. Measurements of linear dichroism on a sample aligned in stretched polyethylene [19] demonstrated the mutually perpendicular polarizations of the two transitions, and suggest the presence of another Si–Si axis polarized transition at higher energies, which density functional theory (DFT) calculations [20] attribute to a $\pi_{Si-C}\pi^*_{Si-C}$ transition (this excitation produces an A_{1u}, an A_{2u}, and an E_u excited configuration). Better calculations are needed for definitive assignments in this higher-energy region.

The two fundamental types of transitions in oligosilanes have thus been illustrated in the simplest case of a single Si–Si bond. In longer oligosilanes, there will be additional σ_{Si-Si} orbitals, but only the highest few will be of any importance for low-energy excitations. There will also be a larger number of σ* and π* orbitals. Because of the lower symmetry, the latter will no longer be degenerate. In order to understand the orbital structure and electronic spectra, we need to examine how the Si–Si bonds in a molecule interact.
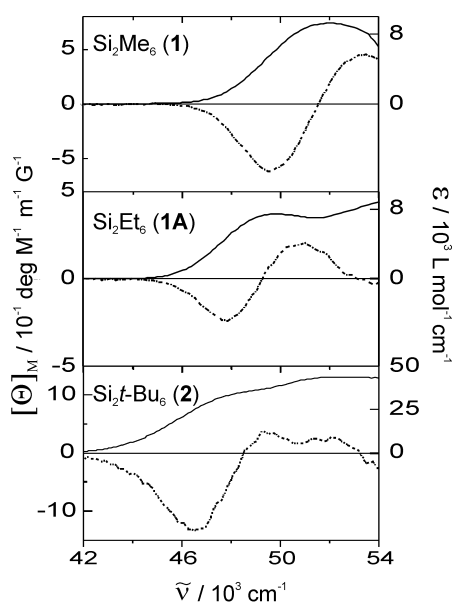
Fig. 2 UV (—) and MCD (- · -) spectra of disilanes **1**, **1A**, and **2** in 3-methylpentane (room temperature).

σ DELOCALIZATION

By itself, the usual representation of saturated molecules by a single Lewis structure implies a complete localization of electrons in noninteracting two-center bond orbitals built from pairs of sp^3 hybrids pointing at each other along the backbone, or from sp^3 hybrid–substituent orbital pairs in the case of lateral bonds. A single valence-bond (VB) structure is ordinarily a good approximation at equilibrium ground-state geometries, but not at transition-state geometries, or when discussing subtle effects such as rotation barriers. When dealing with propagation of spin density or of substituent effects, energy or charge transfer, photoionization, and optical phenomena such as linear and nonlinear polarizability, optical activity, light absorption and emission, etc., this zero-order approximation is also insufficient. In all these and many other situations, it is necessary to consider additional "no-bond" resonance structures in the VB description.

In the molecular orbital (MO) description, σ-bond delocalization is introduced by the inclusion of interaction integrals between two-center σ or σ* bond orbitals in the calculation. A particularly simple picture results when a basis set of sp^3 hybrid orbitals and ls hydrogen orbitals (or analogous orbitals on other substituents) is used, as in the Sandorfy H model [4]. These can be thought of as Weinhold's natural hybrid orbitals (NHOs) [21]. The primary structure of the saturated system is generated when only the primary resonance integrals β_{prim} between orbitals located at neighboring atoms and pointed at each other are considered (Fig. 3). These integrals are large and negative, and produce an in-phase (nodeless) bonding orbital and an out-of-phase (node across bond) antibonding orbital, both strictly localized in one bond. A double occupancy of such a bonding orbital represents a localized σ bond.

To describe σ delocalization, additional smaller integrals need to be considered. Two types of these integrals are particularly important and are sufficient for most purposes (Fig. 3): (i) Geminal resonance integrals β_{gem} between two hybrid orbitals located at the same atom. When the larger lobes of each hybrid are chosen to have the same sign, these integrals are negative, like β_{prim}, but smaller in magnitude. The type of delocalization that they bring about is usually called σ conjugation. The magnitude of β_{gem} is related to the difference in the energy of an s and p atomic orbital and thus also to the singlet–triplet energy difference in a silylene (or carbene). (ii) Vicinal resonance integrals β_{vic} between two
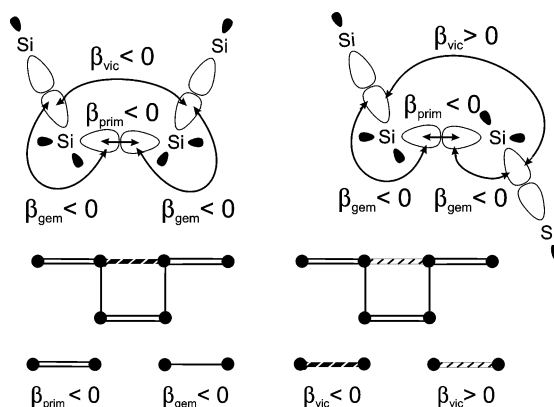
Fig. 3 Top: resonance integrals, β [sign shown for SiSiSiSi dihedral angle smaller (left) and larger (right) than ~100°]. Bottom: isoelectronic interactions in the π systems of dimethylenecyclobutadiene (left) and Möbius dimethylenecyclobutadiene (right).

hybrids located at adjacent atoms but not pointing at each other. Unlike β_{prim} and β_{gem}, the β_{vic} integrals are a function of the angle of rotation about the bond connecting the two silicon atoms. When the larger lobes of each hybrid are chosen to have the same sign, β_{vic} is negative in a syn-periplanar alignment, like β_{prim} and β_{gem}. After a twist of ~100°, β_{vic} increases to zero, and in the anti-periplanar alignment, it is positive. The type of delocalization that the vicinal resonance integrals bring about is usually called σ hyperconjugation (or through-bond coupling). The magnitude of β_{vic} is related to the strength that a π bond between the two atoms would have.

In oligosilanes, β_{gem} is 2–3 times smaller than β_{prim}, and somewhat larger than β_{vic} at the syn-periplanar geometry [22]. The dominance of β_{prim} over the size of the other integrals is responsible for the high degree of localization of σ bonds relative to what one is used to in π systems, where the variation of the magnitude of the resonance integrals is far smaller, even when the double bonds are relatively localized, as in polyenes or polyynes.

Upon going from Si to C, the importance of σ hyperconjugation increases and that of σ conjugation decreases. Upon going from silicon to germanium and further down in the periodic table, the importance of hyperconjugation drops and that of σ conjugation grows. It is, therefore, difficult to say which element yields structures with the most σ delocalization overall, but it follows that the nature of the phenomenon changes as one moves up or down column 14 in the periodic table.

It is clear from Fig. 3 that σ delocalization is always cyclic, even in linear chains (β_{prim}, β_{gem}, β_{vic}, β_{gem} resonance integrals arranged in a series of four-numbered rings), except at the particular conformation at which all SiSiSiSi dihedral angles are close to orthogonal, in which case β_{vic} vanishes. In conformations with smaller dihedral angles, such as gauche, the cyclic subunits of four orbitals interact via four negative resonance integrals and are isoelectronic with ordinary cyclobutadiene, or more closely, dimethylenecyclobutene (Fig. 3). In conformations with larger dihedral angles, such as anti, the cyclic interaction involves three negative and one positive resonance integral, such that the subunits are isoelectronic with Möbius cyclobutadiene (Möbius dimethylenecyclobutene). This difference has a profound effect on the outcome of the cyclic interaction; cf. the antiaromatic ordinary cyclobutadiene and aromatic Möbius cyclobutadiene. Such easy switching between interactions of antiaromatic and aromatic types by a mere change of conformation has no analogy in planar π-electron systems. Closer analysis [22–24] shows that it causes the gap between the highest σ_{Si-Si} and the lowest σ^*_{Si-Si} orbital to be considerably larger in the all-gauche than in the all-anti chain, and that it is responsible for the generally acknowledged "better conjugation" in the latter.

The simple model described above (the "ladder model" of σ-electronic structure) is capable of reproducing the results of full ab initio calculations quite well [22]. For instance, even at the Hückel level,

the values of α_{Si} = –6.20, α_C = –9.28, β_{prim}(SiSi) = –3.55, β_{prim}(Si–C) = –4.22, β_{gem} = –1.65, and β_{vic} = –0.13 – 0.85 cos ω (all in eV), where α_{Si} and α_C are the Coulomb integrals of the sp^3 orbital on Si and of the orbital used by a methyl carbon to attach to the backbone, respectively, reproduce ab initio energies of the bonding orbitals (–10.5 to –8 eV) of a series of several dozen permethylated oligosilanes at a variety of conformations remarkably accurately, with a mean error of 0.03 eV. This is far more accurate than the fit of the latter to experimental ionization potentials, because of the errors inherent in the application of Koopmans' theorem.

CHAIN LENGTH AND σ DELOCALIZATION

Figure 4 shows a comparison of the calculated time-dependent (TD) DFT [B3LYP/6-31G(d)] singlet excitation energies of the lowest three singlet transitions in a series of all-transoid (ω = 165°) permethylated oligosilanes with the absorption spectra observed at low temperatures, where this conformer is believed to dominate. The agreement is remarkably good, considering the approximate nature of the calculations. The intense transition shown in black in the calculated spectra is the first σσ* excitation, and the steady decrease of its calculated and observed energy with the increasing chain length provides a convincing proof that the phenomenon of σ delocalization is real. In the first few members of the series a σπ* excitation, shown in white in Fig. 4, is the lowest. Its energy decreases more slowly with the growing chain length than that of the intense σσ* transition, and from Si_5Me_{12} (6) on, the latter is the lowest. The σπ* transitions are very weak in all cases except Si_2Me_6. As is always the case for σπ* excitations, their transition moments can be thought of as a sum of atomic contributions. The nodal properties of the starting orbital, the σ HOMO (a node at every Si atom) do not match those of the lowest
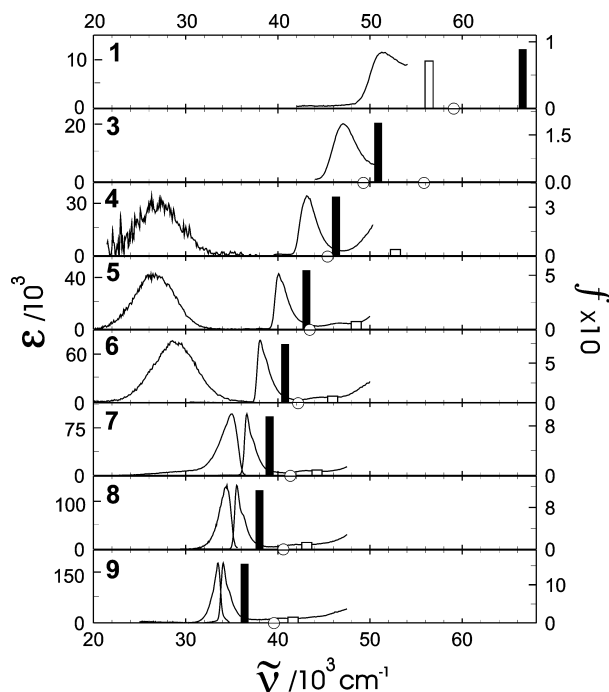

Fig. 4 Calculated [TD B3LYP/6-31G(d)] lowest-energy singlet–singlet σσ* transition (black bar) and two lowest σπ* transitions [white bar; oscillator strength f < 0.01, circle (except in 1 in which the weak transition is to virtual orbitals of mixed nature)], and low-temperature (~77 K) absorption (right) and fluorescence (left) spectra of Me(SiMe$_2$)$_n$Me (n = 2–10) (1, 3–9). Geometries of 1 and 3–6 were fully optimized (MP2/VTZ); those of 7–9 were constructed from MP2/VTZ optimized segments.

π* orbital (no nodes perpendicular to the chain) in any case other than disilane, causing the atomic contributions to the transition moments to be small and to cancel or nearly cancel in a vectorial addition.

The fluorescence spectra, also shown in Fig. 4, are remarkable. For long chains, they are close mirror images of the first absorption band, with a very small Stokes shift, and are clearly Franck–Condon forbidden. Where known, their lifetimes are those expected from integrated absorption intensities. The equilibrium geometries of the ground and excited states are clearly very similar, and the excitation is delocalized throughout the length of the chain. Starting with Si_6Me_{14}, however, the fluorescence spectra change dramatically and become nearly independent of chain length. They are broad, strongly Stokes-shifted and obviously Franck–Condon forbidden. Their lifetimes are longer than expected from integrated intensities [25,26]. In these cases, the equilibrium geometries of ground and excited states are clearly very different.

This behavior has been interpreted using classical exciton theory [27]. The exciton-phonon coupling constant, equal to the ratio of the site distortion energy to the half-width of the exciton band, is much less than unity in the infinite one-dimensional chain, but not zero, causing the exciton to be of the large-diameter type (its length has been estimated at two or three dozen Si–Si bonds) [28,29]. As the chain is shortened, quantum confinement reduces the half-width of the exciton band, causing the coupling constant to increase and the length of the exciton to decrease slowly. When the coupling constant reaches a value close to unity, the size of the exciton is reduced abruptly to approximately one Si–Si bond (small-radius self-trapped exciton).

In more chemical terms, the best the molecule can do to lower its energy starting at the initial ground-state geometry maintained after vertical excitation clearly depends on chain length. When the chain is short and the energy saving by delocalization among the few Si–Si excitation sites available rather small, the stabilization of the excited state by distortion of any one of the Si–Si bond sites is preferable. At the distorted geometries, excitation is localized at the distorted bond and conjugation with the remainder of the chain is weak. Fluorescence is, therefore, nearly independent of chain length. As the chain is extended, a point is reached at which the saving obtained by benefitting from maximum delocalization, available at the original undistorted geometry with all resonance integrals as nearly equal as possible, exceeds the stabilization available from a site distortion. Excited-state relaxation no longer leads to a geometrical distortion, and the geometry of the relaxed excited state changes abruptly.

This explanation is expected to be general: there can be a lower limit as well as an upper limit to chain length that permits fully delocalized conjugation. The concept can be used for other one-dimensional conjugated systems, such as polyenes, in which the site distortion corresponds to a double bond twist. The nonfluorescent twisted state in the localized singlet excitation is favored for the shortest polyenes, whereas the planar state with delocalized singlet excitation is favored for the longer ones, which therefore fluoresce.

The exact nature of the site distortion in the excited state of oligosilanes is not known, but crude calculations [30] suggest that it involves bond stretching as well as valence and SiSiSiSi dihedral angle changes, and mixing of the lowest σσ* and σπ* excitations. For simplicity, we shall refer to it as bond-stretch distortion in the following.

In a finite-length system, the various Si–Si bonds are nonequivalent if they differ by their distance from the chain end. In particular, fluorescence from an excited state localized on the terminal $Me_3Si–SiMe_2$ moiety, which carries five methyl groups, could be detectably different from fluorescence from an excited state localized on one of the internal $Me_2Si–SiMe_2$ moieties, which carry only four methyl groups. In simplest terms, the two excited states are bond-stretch isomers.

Indeed, dual fluorescence has been observed from the localized excited states of Si_5Me_{12} (**5**) [25] and Si_6Me_{14} (**6**) [31] and was attributed to bond-stretch isomers. Up to about 70 K, emission at 29 000 cm^{-1} dominates, whereas above about 100 K, a similar emission shifted to 27 000 cm^{-1} dominates. In the intermediate temperature range, emissions at intermediate energies are observed. The dual fluorescence persists when the hexasilane chain is racked alongside a staffane molecular rod (**19**) [31], making it unlikely that the two fluorescent species are conformational isomers.

Note that the low-temperature absorption and fluorescence excitation spectra of both free-chain Si_6Me_{14} and its racked analog monitored at the emission peak track each other perfectly [31], as expected if a single conformer dominates. At room temperature, this is still true of the [2]staffane racked hexasilane but not of the free-chain hexasilane, which now clearly contains one or more nonemissive conformers absorbing at somewhat shorter wavelengths than the fluorescent one. Comparison of the spectra of the racked and the free-chain species suggests that the low-temperature conformer is essentially the same in both cases. Since in the racked case this can only be a conformer of the all-anti, all-transoid, or a similar extended kind, one can conclude that at low temperatures such a stretched conformation is favored by the free chain hexasilane as well. By analogy to this result, and by reference to computations of conformer energies [32–34], it is then assumed that the low-temperature absorption spectra of all permethylated linear oligosilanes are dominated by similar stretched conformations.

Assuming that one of the emissions originated in a state excited at a terminal Si–Si bond and the other in a state excited at one of the internal Si–Si bonds, we devised a scheme for determining which was which, assuming that the photochemical reaction and fluorescence of oligosilanes occur in competition from the same excited-state minimum. The long-known [35] photochemical abridgement of peralkylated oligosilanes via extrusion of a dialkylsilylene from the silicon chain is believed [31,36–39] to occur by a concerted mechanism in which a new bond forms between the two silicon atoms adjacent to the extruded silicon atom, while the two Si–Si bonds between the forming silylene and the adjacent silicon atoms break, thus producing a silicon chain shorter by one silicon atom and a singlet silylene.

If the two excited states indeed differ by the position of the excited bond in the molecule, and assuming that a silicon atom needs to be located at an excited bond in order to be extruded, the irradiation of permethylated hexasilane at temperatures where one of the fluorescent emissions is observed should result in extrusion of silylene from the terminal bond, while irradiation at temperatures where the other emission is observed should cause extrusion from an internal bond.

The silicon atoms involved in the central bond, Si(3) and Si(4), were each labeled with a single trideuteriomethyl group, thus allowing us to determine which bond is involved in the photochemical reaction. The terminal bond should extrude only unlabeled silylene, the center bond should extrude only labeled silylene, whereas the Si(2)–Si(3) bond should provide a mixture of labeled and unlabeled silylene. Irradiation at temperatures of 37 and 100 K to a low degree of conversion while trapping the silylene with Et_3SiH yielded only products from the extrusion of trideuteriomethyl-labeled silylene from the central Si(3)–Si(4) bond at either temperature. Clearly, at least one of our assumptions was invalid. Either the same Si atom is extruded regardless of which Si–Si bond is excited, or the fluorescence and the photoreaction are not competing, or the dual emission is not due to bond-stretch isomerism, or the whole concept of excitation localization is incorrect.

The attribution of the dual emission to excited bond-stretch isomers seems to be the most likely explanation, but it deserves close scrutiny. For example, could the two fluorescent emissions be due to two different conformations accessible to the molecule in spite of the racking? We are continuing our computational search for additional ground-state conformers, examining the excitation spectrum at different monitoring energies, and synthesizing more tightly racked oligosilanes.

CHAIN CONFORMATION AND σ DELOCALIZATION

The conformations of the parent oligosilanes Si_nH_{2n+2} are similar to those of the alkanes C_nH_{2n+2}, except that the energy difference between the anti and gauche conformation and the barrier between them are smaller. This can be attributed to the larger Si–Si distance and weaker vicinal interactions. However, already in permethylated oligosilanes [32,40,41], and even more so in other peralkylated oligosilanes [42–44] the lateral substituents get into each other's way enough to cause both the gauche and the anti minima to split. As a result, there are three enantiomeric pairs of conformational minima for rotation around an internal Si–Si bond in a permethylated oligosilane chain; in this regard, permethylated

oligosilanes resemble perfluorinated alkanes [45]. The three conformations of a $SiR_2–SiR_2$ bond have been documented experimentally in perchlorotetrasilane [46]. They are the transoid, ortho, and gauche conformations, with dihedral angles of about 165°, 90°, and 55°, respectively. In Si_4Me_{10} (**4**), the gauche and ortho conformers are calculated to be only about 0.2 and 0.6 kcal/mol less stable than the transoid conformer, respectively [32], and the interconversion barriers are all less than 2 kcal/mol. In longer permethylated chains, the number of possible conformers increases rapidly [33,34], and in Si_6Me_{14}, over 30 conformers have been identified computationally (counting a pair of enantiomers as one). Their energies calculated at various levels of approximation such as MP2/DZ can be evaluated easily using a simple set of empirical increments [34].

    Both computational [32,40,47–51] and experimental [32,47,52,53] results for tetrasilanes suggest that the optical properties of oligosilane chains are extremely sensitive to their conformation. New illustrative computational results for permethylated hexasilane are shown in Fig. 5, which shows how the time-dependent (TD) DFT singlet excitation energies for permethylated hexasilane change when the Si–Si backbone is twisted into a regular helix with SiSiSiSi dihedral angles ranging from 180 (all-anti) to 55° (all-gauche). The predicted spectral changes are indeed dramatic. As anticipated from the simple analysis of σ delocalization, the conformations close to the all-anti show the most efficient σ delocalization and the lowest excitation energy.
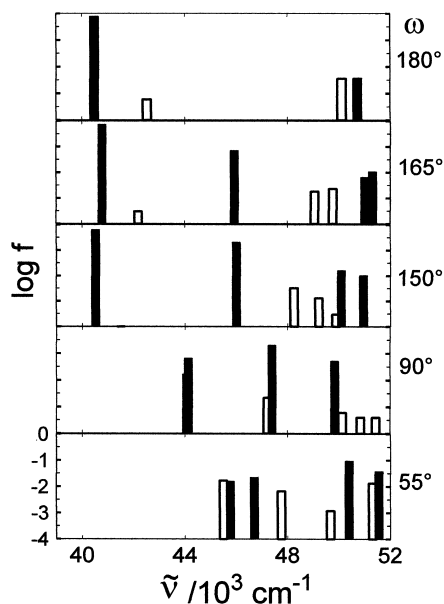

Fig. 5 Calculated [TD B3LYP/6-31G(d)] transition energies and oscillator strengths f for Si_6Me_{14} (**6**) twisted into a regular helix with SiSiSiSi dihedral angles ω of 180 (a, a, a), 165 (t_+, t_+, t_+), 150 (d_+, d_+, d_+), 90 (o_+, o_+, o_+) or 55° (g_+, g_+, g_+). Transitions into B-symmetry (filled) and A-symmetry (hollow) states. The 180 and 150° geometries were optimized (MP2/VTZ) with ω frozen; the others were optimized fully (MP2/VTZ).

    An illustration of the conformational sensitivity of the UV spectra is provided by the most recent experimental results [54]. Figure 6 shows the absorption spectra of a series of peralkylated tetrasilanes constrained by polymethylene chains to conformations with SiSiSiSi dihedral angle ω ranging from 0 to 180° (cf. Chart 1). In all cases, except for **16** and **17**, at least three transitions can be discerned when the absorption and MCD spectra are analyzed.
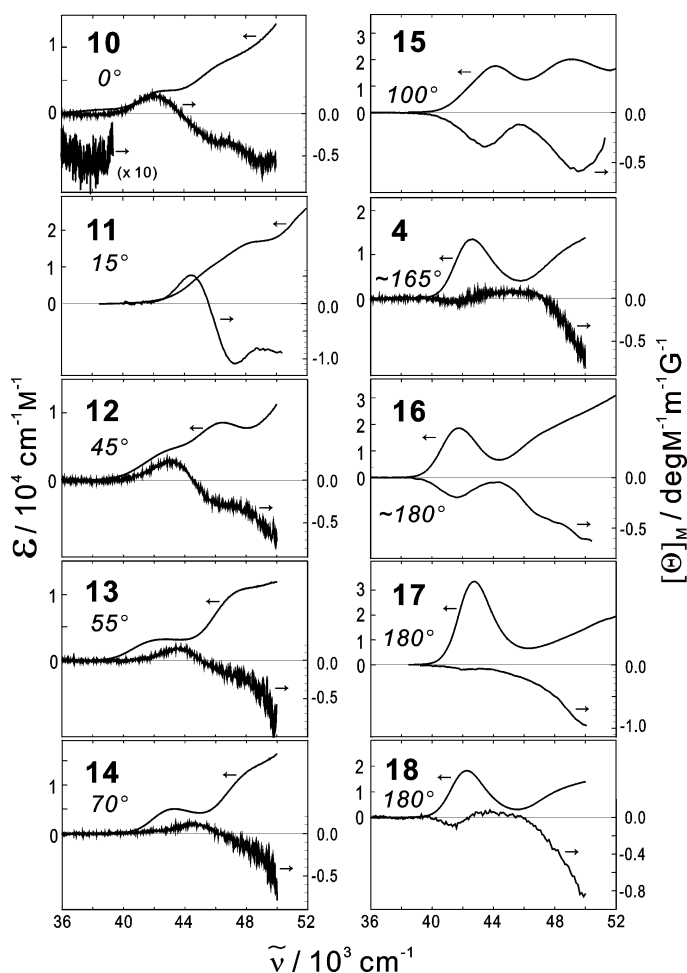
Fig. 6 UV (left axis) and MCD (right axis) room-temperature spectra of tetrasilanes (**4**, **10–18**) in alkane solvents. Calculated SiSiSiSi angles ω in italics.

It is striking that in Fig. 6 there is hardly any change in the excitation energies of the tetrasilane chromophores as its dihedral angle ω is varied from 0 to 180°, and that it is primarily the intensity of the three most clearly observed transitions that undergoes dramatic changes. Does this mean that the simple concepts concerning σ delocalization that we developed in the section "σ Delocalization", based on the ladder C model [22–24], break down? After all, they suggest that σσ* excitation occurs at lower energies in the better-conjugated anti conformation than in the gauche or syn conformations. An answer is provided by theoretical work quoted above, which contains excited-state correlation diagrams for ω ranging from 0 to 180° at low levels of ab initio theory [40,47,48] and results for individual conformers obtained in high-quality calculations [49–51]. The latter results are approximated by TD DFT, which has been used to obtain the correlation diagram shown in Fig. 7. The calculated energies (line location) and intensities (line thickness) of the six lowest electronic transitions in Si_4Me_{10} are displayed as a function of the dihedral angle ω and agree with observed trends displayed in Fig. 6. Of the six excited states, three are of B and three are of A symmetry. The latter are polarized perpendicular to the chain direction and would be expected to carry little intensity. At the planar anti (ω = 180°) and syn (ω = 0°) geometries, additional state symmetry classification is possible, and orbitals of σ and π symmetries can be rigorously distinguished.
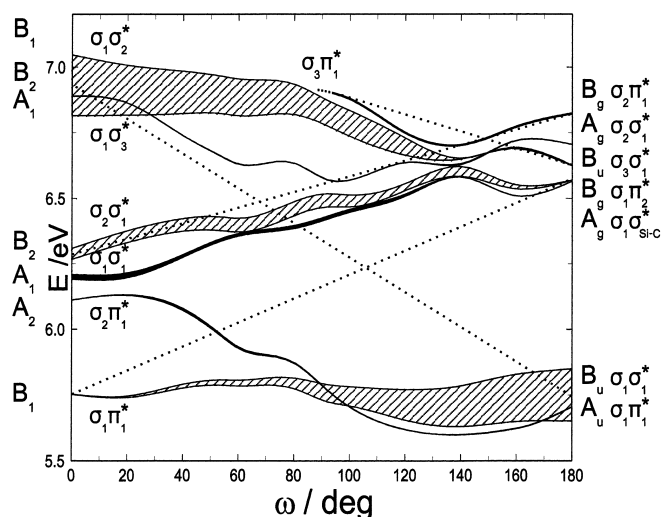
Fig. 7 State correlation diagram for Si_4Me_{10} (**4**) as a function of the SiSiSiSi dihedral angle ω [TD B3LYP/6-31G(d)//MP2/VTZ]. A-symmetry transitions (black); B-symmetry transitions (hatched). Transition energies are shown as midpoints of each strip; intensities are proportional to strip thickness. The oscillator strength of the lowest-energy B_u state at 180° is 0.4. Intended correlation of B symmetry states (···).

We consider states of B symmetry first. At the anti geometry, the $\sigma_1\sigma_1^*$ (HOMO to LUMO) transition into the B_u state is low in energy (we label the orbitals in the order of energy, starting at the Fermi level). As anticipated from its analogy to the HOMO → LUMO transition in a polyene, which also adds one node, the $\sigma_1\sigma_1^*$ transition carries large intensity. About 1 eV higher, there is a $\sigma_1\pi_2^*$ transition into a state of B_g symmetry, which has zero intensity. In the syn limit, the $\sigma_1\sigma_1^*$ and the $\sigma_1\pi_2^*$ transitions have exchanged positions, and now the former is ~1 eV higher. Because the virtual orbitals change their order upon going from one to the other limit, the transition labeled $\sigma_1\sigma_1^*$ on the right is labeled $\sigma_1\sigma_2^*$ on the left in Fig. 7. The intended correlation is shown as a dotted line. In the syn limit, the transition is of B_2 symmetry and is still very intense. The B_g transition that is labeled $\sigma_1\pi_2^*$ in the anti limit is labeled $\sigma_1\pi_1^*$ in the syn limit. It is of B_1 symmetry in the syn limit and has almost no intensity at any dihedral angle. The large decrease in the energy of the σσ* configuration upon going from the syn to the anti conformation is exactly as expected from the ladder C model. Since in this model the lateral bonds are not included, there are no π-symmetry orbitals and hence no σπ* states. One would then indeed predict one intense low-energy transition of the σσ* type, and would expect it to be strongly red-shifted on going from the syn to the anti conformer.

In the ladder H model, and in all better descriptions, the lateral bonds are considered. Now, there will be π-symmetry orbitals and σπ* transitions, and in short chains such as Si_4Me_{10} they are in a similar energy region as the lowest $\sigma_1\sigma_1^*$ transition. It turns out that the excitation energy of the lowest σπ* transition to a state of B symmetry described above decreases strongly upon going from the anti to the syn conformer for reasons that are readily apparent upon closer inspection of the form of the MOs within the framework of the ladder H model. This causes the intended crossing of the σσ* and σπ* states of B symmetry shown in the anti–syn correlation diagram in Fig. 7 and described above. Since at nonplanar geometries the rigorous distinction between σ and π orbitals disappears, and both states are of the same B symmetry in the C_2 group, this crossing is avoided. It is avoided so strongly that the energy of the lower of the two resulting states, which connects the syn B_1 with the anti B_u state, is virtually independent of the dihedral angle, and that of the upper one, which connects the syn B_2 state with the anti B_g state, changes only moderately. Only a gradual shift of intensity from the upper to the lower

state as the geometry changes from syn to anti testifies to the presence of the originally intended crossing. This is the interpretation described in earlier work [32,40,47,48].

The behavior seen in Fig. 7 is even more complicated in that at the TD DFT level of calculation two additional B states get involved, producing two additional weakly avoided crossings. A lower-energy B_2 state is now inserted at the syn geometry at about 6.3 eV. It is described as a $\sigma_2\sigma_1^*$ excitation from the HOMO–1 level. It increases in energy as the geometry changes to anti, undergoes a weakly avoided crossing with the previously described B_2(syn)–B_g(anti) state, and another weakly avoided crossing with a high-energy B symmetry state that has not been mentioned so far. It ends up as a second B_g ($\sigma_2\pi_1^*$) state of the anti conformer. The steep rise of energy of this state with increasing dihedral angle is understandable, in view of the well-documented [18] concurrent stabilization of the HOMO-1 orbital σ_2. The high-energy B symmetry state involved in the avoided crossing mentioned last is the second B_u state at the anti geometry, which involves an excitation from the HOMO-2 orbital and rises steeply as the dihedral angle decreases.

The three states of A symmetry, two $\sigma\sigma^*$ and one $\sigma\pi^*$, go through a similar exercise, but none of them is expected to have much intensity at any dihedral angle. Only the second of the three excited A states, calculated to carry more oscillator strength than the others, is observed in the experimental spectra. It is located between the lower two B states, and has detectable intensity only at small dihedral angles. The trends expected qualitatively from the simple ladder model are thus actually borne out.

Conformational effects on the low-energy region in the spectra of longer oligosilanes with few strong twists is expected to be simpler, since the lowest $\sigma\sigma^*$ excitation energies can now be expected to be well below the lowest $\sigma\pi^*$ excitation energies, minimizing the occurrence of intended crossings between them. The expectations based on the ladder C model should then be fulfilled. However, there is no free lunch: now, the number of low-energy conformers is much higher and their spectral assignments will be very difficult to obtain.

CONFORMERS OF PERMETHYLATED HEPTASILANE

We have selected Si_7Me_{16} (**7**) for a detailed study, since this is the shortest chain in which some conformers, but not all, exhibit Franck–Condon allowed fluorescence. We estimate the number of stable conformers at well over a hundred, counting an enantiomeric pair as one, with possibly only a dozen or two at very low energies. It is an interesting challenge to identify at least a few of them computationally and experimentally in a complex mixture. Realistically, we can only hope to identify and assign the most intense electronic transitions in each.

The increment method described earlier [34] produced a list of candidates for low-energy conformers. Their predicted energies (Table 1) are probably quite reliably equal to energies that would be computed at the MP2/6-31G(d) level, but there are two problems with these numbers. First, oligosilane geometries are not predicted reliably until the MP2/TZ level, and this is likely to affect the relative energies of conformers, which are influenced considerably by intersubstituent interactions. Second, the computed energies are for molecules isolated in the gas phase, and there could be differential solvent effects, since the accessible surface areas of compact and extended conformations will be quite different.

We are, therefore, repeating the determination of conformation increments at the MP2/TZ level of theory, and we are including solvation energies using Truhlar's approximation [55,56]. Using scaled frequencies obtained at a lower level of theory, we are also including zero point energies, rotational and vibrational entropy, and heat capacity contributions in order to derive increments for relative conformer free energies. The search for optimal values of these parameters is based on least squares fitting for several dozen conformations of Si_4Me_{10}, Si_5Me_{12}, and Si_6Me_{14} that were identified in previous work [34] as critical for getting the best increments for fitting ab initio data.

Table 1 Conformers of Si_7Me_{16} (**7**): Calculated relative ground-state energies (kcal/mol), and calculated and observed first transition energies (cm^{-1}).

Conformer	Ground-state energy		Transition energy	
	E''_{incr} HF/3-21G(d) //HF/3-21G(d)[a]	E^0_{incr} MP2(fc)/6-31G(d) //HF/3-21G(d)[b]	TD B3LYP/6-31G(d) //MM3	Obsd.
$t_+t_+t_+t_+$	0.00	0.00	37 820	36 700
$t_+t_+t_-t_-$	0.71	0.85	37 530	36 400
$t_+at_-t_-$[c]	——	——	37 590	~36 500
$t_+t_+t_+g_+$	0.77	0.19	39 330	~37 500
$t_+t_+g_+t_+$	0.87	0.23	41 060	~39 000
$t_+t_+t_+o_-$	0.99	0.66	38 910	~37 000
$t_+t_+o_-t_+$	1.07	0.75	39 850	~38 100
$g_+t_+t_+g_+$	1.55	0.38	41 560	~40 500
$t_+g_+t_+g_+$	1.65	0.42	43 620; 45 690[d]	
$t_+g_+t_+o_-$	1.86	0.89	42 660	
$o_+t_-t_-o_+$	1.97	1.32	39 860	
$t_+t_+g_+g_+$	1.98	0.77	41 940	

[a]Calculated by the increment method [32] at the HF/3-21G(d)//HF/3-21G(d) level.
[b]Calculated by the increment method [32] at the MP2(fc)/6-31G(d)//HF/3-21G(d) level.
[c]The ground-state energy of the $t_+at_-t_-$ conformer is not a minimum on the ground-state potential energy surface at the levels available using the increment method.
[d]The second transition energy is also listed when its oscillator strength exceeds 0.2.

In addition to a prediction of relative free energies of the most stable conformers, we need predictions of their UV spectra. Results such as those shown in Fig. 4 encourage us to believe that the TD B3LYP/6-31G(d) method is probably capable of rendering correctly the relative energies of the most intense transitions of the individual conformers of Si_7Me_{16}, and we are presently checking its performance for a series of conformationally constrained tetrasilanes. Assuming that the outcome will be positive, we have listed in Table 1, and shown in Fig. 8, the predicted positions of the first intense band or two for each of the Si_7Me_{16} conformers listed. Comparison with experimental transition energies so far
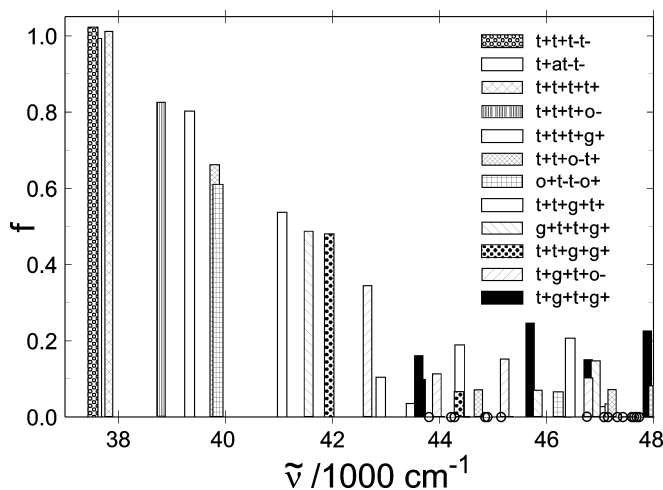

Fig. 8 Calculated [TD DFT B3LYP/6-31G(d)//MM3] energy and oscillator strength for the lowest three transitions of the nine lowest ground-state energy conformers of Si_7Me_{16} (**7**) at the HF/3-21G(d)//HF/3-21G(d) level [32], plus three additional conformers. Hollow circles indicate very low intensity transitions.

suggests the calculated energies are too high by 1100–2000 cm^{-1}, which would be the same as in the case of the all-transoid conformers of a whole series of oligosilane chains [20].

  With the expected relative free energies and relative spectral transition energies and strengths in hand, we can turn to an interpretation of the experimental data obtained on Si_7Me_{16} conformer mixtures. To improve our chances of extracting the spectral properties of individual conformers correctly, we have added two peralkylated heptasilanes whose conformational balance has been modified by racking on an [n]staffane rod as explained above for shorter oligosilanes. A set of MM3 geometry optimizations using the simulated annealing technique [57–60] has produced a short list of likely conformations for the heptasilane chain racked on [2]staffane (20), where it is forced to be bent, and on [3]staffane (21), where it is forced to be quite extended. The results are summarized in Tables 2 and 3, respectively, and the lowest-energy conformations of 20 and 21 are shown in Fig. 9.

Table 2 Conformers of racked Si_7 (20) and Si_7Me_{16} (7): Calculated relative ground-state energies (kcal/mol), calculated first transition energies of 7, and observed transition energies of 20 (cm^{-1}).

Conformer	Ground-state energy	Transition energy	
	ΔE_{MM3} (kcal/mol) 20	TD B3LYP/6-31G(d) //MM3 of Si_7Me_{16} 7	Obsd. 20
$o_+t\_t\_o_+$	0.0	39 860	38 100
$t_+t_+t_+g_+$	0.5	39 330	~37 500
$d_+t_+t_+g_-$	1.0		
$d_+g_+t\_g_-$	1.0	~42 670	
$g_+t_+t_+g_+$	1.2	41 560	~40 500
d_+t_+a/t_g_-	1.3		
$o_+t\_t\_g_+$	1.5		
$t_+o\_o\_t_-$	1.7		
$t_+t_+d_+o_-$	2.2		
$t_+at\_t\_^a$	———	37 530	36 300

[a]The ground-state energy of the $t_+at\_t\_$ conformer of 20 is not a minimum at the MM3 level. However, experimental data indicate that the molecule can access this, or a similar, conformation.
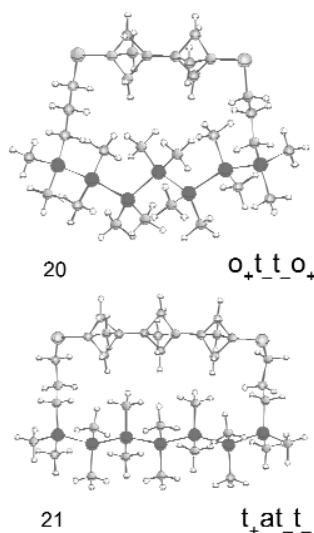

20   o₊t_t_o₊

21   t₊at_t_

Fig. 9 The lowest-energy structures calculated (MM3) for 20 (top) and 21 (bottom).

Table 3 Conformers of racked Si_7 (**21**) and Si_7Me_{16} (**7**): Calculated relative ground-state energies (kcal/mol), calculated first transition energies of **7** and observed transition energies of **21** (cm^{-1}).

Conformer	Ground-state energy	Transition energy	
	ΔE_{MM3} **21**	TD B3LYP/6-31G(d) //MM3 of Si_7Me_{16} (**7**)	Obsd. **21**
$t_+a_+t\_t\_$ [a]	0.0	37 590	36 500
$t_+at_+t_+$	0.0		
$t_+t/a\_t\_t\_$	0.2		
$a_+t\_t\_t\_$ [b]	0.3		
$t_+t\_t\_t\_$	0.5	37 530	~36 400
$a/t_+t\_t\_t\_$	0.5		
$t/a_+t_+t/a_+t_+$	0.6		
$a/t_+t_+t_+t_+$	0.8	37 820	
$t_+a/t\_t\_o_+$	1.8	38 910	~37 000
$t_+o\_t_+o_+$	2.2		
$t_+at_+t_+$	2.3		

[a] Another conformer with the same conformation of the Si backbone chain is located 2.0 kcal/mol higher in energy at the MM3 level.
[b] Another conformer with the same conformation of the Si backbone chain is located 0.4 kcal/mol higher in energy at the MM3 level.

The experimental data that have been obtained so far are the temperature-dependent UV absorption spectra of Si_7Me_{16} (Fig. 10) and each of its two racked analogs (Fig. 11), and their fluorescence and fluorescence excitation spectra obtained at various excitation and monitoring energies (Figs. 12–14). Only some of the conformers are luminescent. This is a blessing, since the problem of disentangling their properties is simplified, and a curse, since one finds out nothing about some of the most interesting conformers. Judicious choice of excitation wavelength permits partially selective excitation
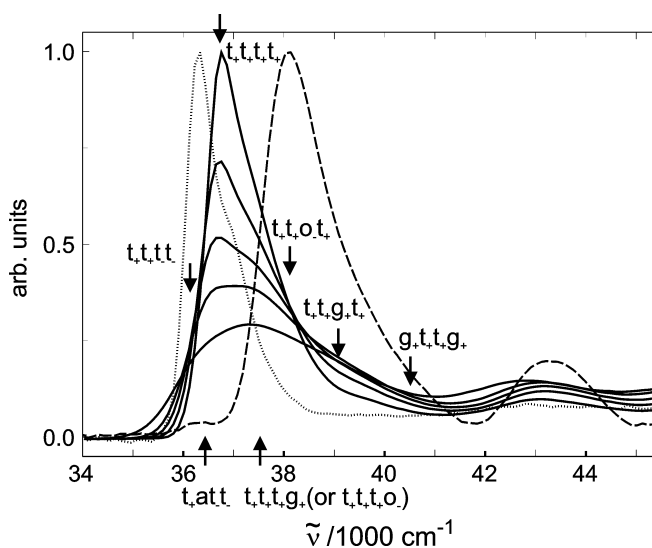

Fig. 10 UV absorption curves in cyclo/isopentane (3:7 by volume) normalized to unity at room temperature: Si_7Me_{16} (**7**) at RT, 193, 153, 120 and 89 K (—, from bottom to top, corrected for solvent contraction); **21** (- - -) and **22** (···) at 77 K. Conformer assignments are indicated.
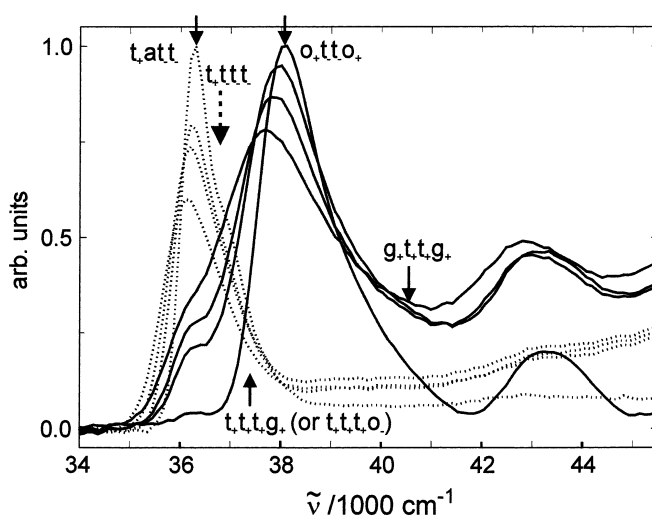
Fig. 11 UV absorption curves in cyclo/isopentane (3:7 by volume) normalized to unity at room temperature: **20** (—) and **21** (⋯) at 198, 148, 123, and 77 K (from bottom to top, corrected for solvent contraction). Conformer assignments are indicated; dashed arrow indicates assignment only to **21**.
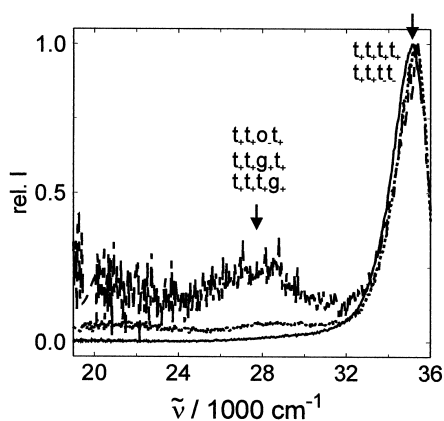

Fig. 12 Emission spectra in cyclo/isopentane (3:7 by volume): Si_7Me_{16} (**7**) at 77 K. Conformer assignments are indicated. Excitation energy: (- - -) 39 230 cm^{-1}, (⋯) 38 310 cm^{-1}, (—) 36 230 cm^{-1}.

of one or another conformer, and judicious choice of monitoring wavelength permits partially selective detection of the emission from one or another conformer. A combination of many experiments of this kind permitted us to detect a minimum of seven distinct conformers contributing to the spectral properties of Si_7Me_{16}, three contributing to the [3]staffane racked heptasilane, nearly identical in their spectral properties to three of those of Si_7Me_{16} and, thus, presumably corresponding to the same or very similar conformations, and four contributing to the [2]staffane racked heptasilane, three of them nearly identical in their spectra to those of Si_7Me_{16} and thus also likely to have very similar conformations, but one being very distinctly different. We have two independent tools for identifying the eight structures: Comparison of the temperature dependence of the contributions to the spectra from the eight individual conformers that have been identified with the computed free energies, and comparison of the relative positions of their intense peaks with the computed spectra. The results are shown in Tables 1–3 and Figs. 10–14 and are still only tentative. In order to confirm them, we intend to perform a global
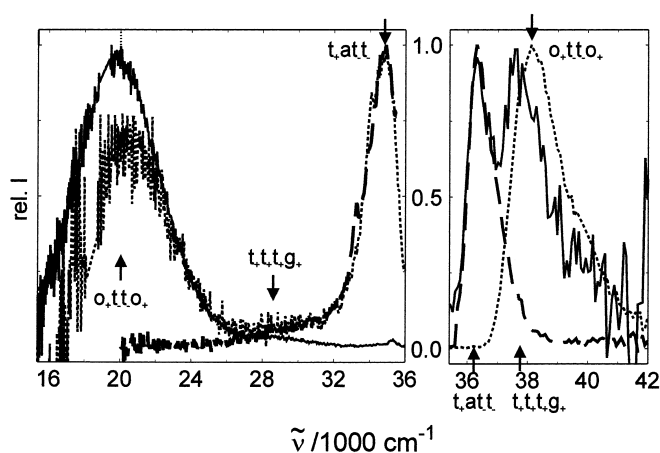
Fig. 13 Emission (left) and excitation (right) spectra in cyclo/isopentane (3:7 by volume): **20** at 77 K. Conformer assignments are indicated. Excitation energy: (—) 38 310 cm^{-1}, (···) 37 040 cm^{-1}, (- - -) 36 230 cm^{-1}; emission energy monitored: (- - -) 34 840 cm^{-1}, (—) 31 250 cm^{-1}, (···) 20 000 cm^{-1}.
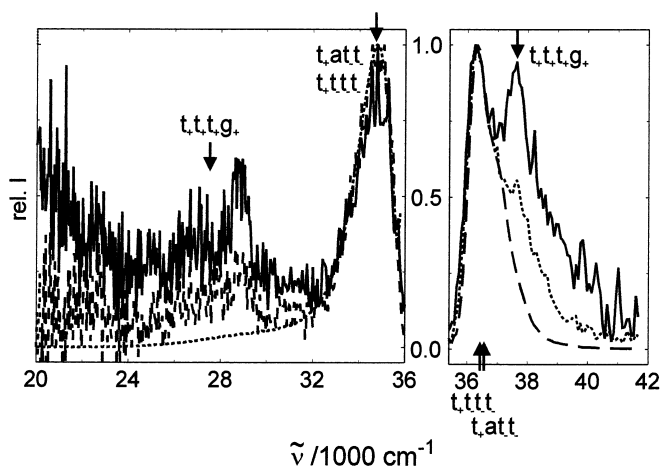

Fig. 14 Emission (left) and excitation (right) spectra in cyclo/isopentane (3:7 by volume): **21** at 77 K. Conformer assignments are indicated. Excitation energy: (—) 39 810 cm^{-1}, (- - -) 38 310 cm^{-1}, (···) 36 230 cm^{-1}; emission energy monitored: (- - -) 34 840 cm^{-11}, (···) 27 780 cm^{-1}, (—) 25 000 cm^{-1}.

analysis of the fluorescence lifetimes at various wavelengths of excitation and detection. The construction of an appropriate spectrometer is currently underway.

A MYSTERIOUS LOW ENERGY EMISSION

All is well that ends well, and it would not be good to end on a note that indicates that all problems in the electronic spectroscopy of oligosilanes have been solved or are on their way to being solved, as this would threaten the employment opportunities of future photophysicists. Indeed, we are currently very puzzled by a very low energy emission that we have observed for several of the oligosilanes. As described above, the chains longer than Si_7Me_{16}, and the extended conformers of Si_7Me_{16}, emit a Franck–Condon allowed fluorescence with a small Stokes shift from a delocalized excited state, at energies very close to their first strong absorption maximum. The shorter chains, and some of the twisted

conformers of Si_7Me_{16}, emit from a lower-energy localized excited state at about $28\,000$ cm^{-1}, and this emission is nearly the same regardless of the length of the chain, in keeping with the localized nature of the excited state. The largest variations we have observed are about 3000 cm^{-1}.

Now, for several conformers of several chain lengths, most of them twisted, including the lowest-energy conformation of **20**, we have observed a strong emission at $20\,000$ cm^{-1}, and believe that we have eliminated the possibility that it might be due to impurities. This emission could be due to some even more severely distorted excited state with localized excitation, or it could be due to phosphorescence, and we are currently trying to assign it.

SUMMARY

Our survey covered a considerable stretch of territory. We started by providing some motivation for the study of electronic states of saturated systems of σ bonds and explained why we have focused on oligosilanes. We then described the nature of σ-electron delocalization in simple terms and emphasized its intrinsically cyclic nature, even in linear chains. We considered the effects of chain length and emphasized the generality of the existence of both lower and upper length limits for complete exciton delocalization in a finite chain. We then turned to the effects of chain conformation. There is generally a larger variety of favored conformations in chains whose lateral substituents are larger than hydrogens, as is the case in peralkylated oligosilanes, complicating the analysis of their properties. For an understanding of the effect of chain conformation on electronic states, the backbone-only ladder C model, with its emphasis on the aromatic vs. antiaromatic cyclic interactions dictated by chain conformation, provides a good starting point. However, in the shorter chains, in which σπ* states are competitive with σσ* states in energy, they introduce complications that cannot be ignored, and their consideration requires at least the ladder H level of treatment, which explicitly includes the orbitals of the lateral bonds. Standard TD DFT theory appears quite promising for predicting the spectra of oligosilanes. Finally, we have described our efforts to separate the spectral properties of the numerous individual conformers of heptasilanes on the way to a general understanding of the relations between conformation and electronic structure. We have also described a new very low-energy emission from several oligosilane conformers, which remains unassigned.

ACKNOWLEDGMENTS

REFERENCES

1. J. Michl. *Top. Curr. Chem.* **46**, 1 (1974).
2. S. L. Wallace and J. Michl. In *Photochemistry and Photobiology*: Proceedings of the International Conference, January 10, 1983, University of Alexandria, Egypt; A. H. Zewail (Ed.), Vol. II, p. 1191, Harwood Academic, Chur, Switzerland (1983).
3. F. Hirayama and S. Lipsky. *J. Chem. Phys.* **51**, 3616 (1969).
4. C. Sandorfy. *Can. J. Chem.* **33**, 1337 (1955).
5. R. D. Miller and J. Michl. *Chem. Rev.* **89**, 1359 (1989).
6. J. Michl and R. West. In *Silicon-Containing Polymers: The Science and Technology of their Synthesis and Applications*, R. G. Jones, W. Ando, J. Chojnowski (Eds.), p. 499, Kluwer, Dordrecht (2000).
7. T. J. Drahnak, J. Michl, R. West. *J. Am. Chem. Soc.* **101**, 5427 (1979).
8. R. West, M. J. Fink, J. Michl. *Science* **214**, 1343 (1981).
9. A. G. Brook, F. Abdesaken, B. Gutekunst, G. Gutekunst, R. K. Kallury. *J. Chem. Soc., Chem. Commun.* 191 (1981).

10. S. Hayase. *Prog. Polym. Sci.* **28**, 359 (2003).
11. R. West. In *Chemistry of Organic Silicon Compounds*, Z. Rappoport and Y. Apeloig (Eds.), p. 541, Wiley, Chichester (2001).
12. N. Matsumoto, H. Suzuki, H. Miyazaka. In *Silicon-Containing Polymers*, R. Jones, W. Ando, J. Chojnowski (Eds.), p. 531, Kluwer, Dordrecht (2000).
13. R. D. Miller, D. Hofer, J. F. Rabolt, G. N. Fickes. *J. Am. Chem. Soc.* **107**, 2172 (1985).
14. J. Michl. *Acc. Chem. Res.* **23**, 127 (1990).
15. M. B. Robin. *Higher Excited States of Polyatomic Molecules*, Vol. 1, p. 189, Academic, New York (1974).
16. A. D. Becke. *J. Chem. Phys.* **98**, 5648 (1993).
17. R. Stowasser and R. Hoffmann. *J. Am. Chem. Soc.* **121**, 3414 (1999).
18. H. A. Fogarty, D. E. David, C.-H. Ottosson, J. Michl, H. Tsuji, K. Tamao, M. Ehara, H. Nakatsuji. *J. Phys. Chem. A* **106**, 2369 (2002).
19. D. L. Casher, H. Tsuji, A. Sano, M. Katkevics, A. Toshimitsu, K. Tamao, M. Kobota, T. Kobayashi, C. H. Ottosson, D. E. David, J. Michl. *J. Phys. Chem. A*. **107**, 3559 (2003).
20. D. W. Rooklin, T. Schepers, M. K. Raymond-Johansson, J. Michl. *Photochem. Photobiol. Sci.* **2**, 511 (2003).
21. A. E. Reed, L. A. Curtiss, F. Weinhold. *Chem. Rev.* **88**, 899 (1988).
22. T. Schepers and J. Michl. *J. Phys. Org. Chem.* **15**, 490 (2002).
23. H. S. Plitt and J. Michl. *Chem. Phys. Lett.* **198**, 400 (1992).
24. H. S. Plitt, J. W. Downing, M. K. Raymond, V. Balaji, J. Michl. *J. Chem. Soc. Faraday Trans.* **90**, 1653 (1994).
25. M. K. Raymond. Ph.D. dissertation, University of Colorado, Boulder, CO (1997).
26. Y.-P. Sun and J. Michl. *J. Am. Chem. Soc.* **114**, 8186 (1992).
27. M. K. Raymond and J. Michl. *Int. J. Quant. Chem.* **72**, 361 (1999).
28. J. Michl, J. Downing, T. Karatsu, K. A. Klingensmith, G. M. Wallraff, R. D. Miller. In *Inorganic and Organometallic Polymers*, M. Zeldin, K. Wynne, H. Allock (Eds.), ACS Symposium Series 360, Chap. 5, p. 61, American Chemical Society, Washington, DC (1988).
29. J. R. G. Thorne, S. A. Williams, R. M. Hochstrasser, P. J. Fagan. *Chem. Phys.* **157**, 401 (1991).
30. H. Teramae and J. Michl. *Chem. Phys. Lett.* **276**, 127 (1997).
31. S. Mazières, M. K. Raymond, G. Raabe, A. Prodi, J. Michl. *J. Am. Chem. Soc*. **119**, 6682 (1997).
32. B. Albinsson, H. Teramae, J. W. Downing, J. Michl. *Chem. Eur. J.* **2**, 529 (1996).
33. B. Albinsson, D. Antic, F. Neumann, J. Michl. *J. Phys. Chem. A* **103**, 2184 (1999).
34. C. H. Ottosson and J. Michl. *J. Phys. Chem. A* **104**, 3367 (2000).
35. M. G. Steinmetz. *Chem. Rev.* **95**, 1527 (1995).
36. B. G. Ramsey. *J. Organomet. Chem.* **67**, C67 (1974).
37. H. Sakurai, Y. Kobayashi, Y. Nakadaira. *J. Am. Chem. Soc.* **96**, 2656 (1974).
38. J. Michl and V. Balaji. In *Computational Advances in Organic Chemistry*, C. Ögretir and I. G. Csizmadia (Eds.), p. 323, Kluwer, Dordrecht (1991).
39. A. Venturini, T. Vreven, F. Bernardi, M. Olivucci, M. A. Robb. *Organometallics* **14**, 4953 (1995).
40. H. Teramae and J. Michl. *Mol. Cryst. Liq. Cryst*. **256***, 149 (1994).
41. F. Neumann, H. Teramae, J. W. Downing, J. Michl. *J. Am. Chem. Soc*. **120**, 573 (1998).
42. H. A. Fogarty, C. H. Ottosson, J. Michl. *J. Mol. Struct.* (*Theochem.*) **506**, 243 (2000).
43. H. A. Fogarty, C. H. Ottosson, J. Michl. *J. Mol. Struct.* (*Theochem.*) **556**, 105 (2000).
44. J. Michl and R. West. *Acc. Chem. Res.* **33**, 821 (2000).
45. B. Albinsson and J. Michl. *J. Phys. Chem.* **100**, 3418 (1996).
46. R. Zink, T. F. Magnera, J. Michl. *J. Phys. Chem. A* **104**, 3829 (2000).
47. B. Albinsson, H. Teramae, H. S. Plitt, L. M. Goss, H. Schmidbaur, J. Michl. *J. Phys. Chem.* **100**, 8681 (1996).
48. R. Crespo, H. Teramae, D. Antic, J. Michl. *Chem. Phys*. **244**, 203 (1999).

49. R. Crespo, M. Merchán, J. Michl. *J. Phys. Chem. A* **104**, 8593 (2000).
50. M. C. Piqueras, M. Merchán, R. Crespo, J. Michl. *J. Phys. Chem. A* **106**, 9868 (2002).
51. M. C. Piqueras, R. Crespo, J. Michl. *J. Phys. Chem. A*. **107**, 4661 (2003).
52. R. Imhof, H. Teramae, J. Michl. *Chem. Phys. Lett.* **270**, 500 (1997).
53. H. Tsuji, A. Toshimitsu, K. Tamao, J. Michl. *J. Phys. Chem. A* **105**, 10246 (2001).
54. H. Tsuji, H. Fogarty, R. Imhof, P. Rempala, K. Tamao, J. Michl. In preparation.
55. P. Winget, J. D. Thompson, C. J. Cramer, D. G. Truhlar. *J. Phys. Chem. A* **106**, 5160 (2002).
56. M. Dupuis, A. Marquez, E. R. Davidson. HONDO 99.6, 1999, based on HONDO 95.3; M. Dupuis, A. Marquez, E. R. Davidson, Quantum Chemistry Program Exchange (QCPE), Indiana University, Bloomington, IN 47405; HONDO/S-v.3.4, by J. D. Xidos, J. L. Thompson, T. Z. Hawkins, B. J. Lynch, Y. Volobuev, D. Rinaldi, D. A. Liotard, C. J. Cramer, D. G. Truhlar, University of Minnesota, Minneapolis, 2001, based on HONDO-v.99.6.
57. J.-H. Lii and N. L. Allinger. *J. Comp. Chem.* **19**, 1001 (1998).
58. J.-H. Lii and N. L. Allinger. *J. Comp. Chem.* **7**, 591 (1994).
59. M. Saunders. *J. Comp. Chem.* **10**, 203 (1989).
60. M. Saunders. *J. Am. Chem. Soc.* **109**, 3150 (1987).